IJE TRANSACTIONS C: Aspects Vol. 33, No. 6, (June 2020) 1105-1113

International Journal of Engineering

Journal Homepage: www.ije.ir

Improving 3-D Imaging Breast Cancer Diagnosis Systems Using a New Method for Placement of Near-infrared Sources and Detectors

Y. Noori shirazi[a], A. Esmaeli*[b], M. B. Tavakoli[a], F. Setoudeh[c]

[a] *Electrical Engineering Department, Arak Branch, Islamic Azad University, Arak, Iran*
[b] *Plasma and Nuclear Fusion Research School, Nuclear Science and Technology Research Institute, Tehran, Iran*
[c] *Department of Electrical Engineering, Arak University of Technology, Arak, Iran*

P A P E R I N F O

Paper history:
Received 13 August 2019
Received in revised form 12 March 2020
Accepted 13 April 2020

Keywords:
Optical Imaging System
Near-infrared
Abnormal Area
Sources And Detectors
Breast Cancer Diagnosis

A B S T R A C T

The objective of this research is to improve the 3-D imaging system using near-infrared light emission in breast tissue to achieve a more accurate diagnosis of the tumor. Experimental results in this research on this imaging system indicate that a more accurate diagnosis of abnormal areas depends on the location of the sources and detectors. Therefore, an improved location model has been proposed to determine a more suitable placement of sources and detectors. In this article, no human breast cancer samples were examined due to inaccessibility to a 3-D imaging system using near-infrared lights. Since such experiments should be conducted several times to obtain more accurate reconstructed images, the proposed method was evaluated using the optical images reconstruction toolbox of NIRFAST 7.2 in the MATLAB programming environment. The results were then compared with the results of similar articles. The obtained results showed that the proposed placement of sources and detectors can detect abnormal areas with a much lower error rate. Furthermore, the proposed placement of sources and detectors achieved a good result in simultaneously diagnosing two abnormal areas.

***doi**: 10.5829/ije.2020.33.06c.07*

NOMENCLATURE

MRI	Magnetice resonance imaging	z	Standard normal	$x^* = \mu + Z_\beta\sigma$	Random variable
CT	Computed tomography	**Greek Symbols**		**Subscripts**	
PET	Posityon emission tomography	μ	Average	*Z*	Height
P	Probability	W_1, W_2, W_3	Coefficient	*mm*	Milimeter
μa	Absorption coefficient	$\beta = \frac{w_2}{w_2 - w_3}$	Coefficient	*N*	Newton
μs	Scattering coefficient				
E	Expected value	σ	Standard deviation		
$E(\delta)$	Expected value of variations	Z_β	Confidence interval		

1. INTRODUCTION

Breast cancer is one of the most common and dangerous diseases among women which has emerged as a challenging problem in all societies. Quick diagnosis can significantly influence its prompt treatment and control of breast cancer, and can reduce mortality among women [1]. Currently, mammography is the most common imaging system for diagnosing tumor. It provides high-resolution images for diagnosing abnormal areas in breast tissue [2]. In conventional mammography [3, 4], the breast is pressurized between two plates, one of which is a film and the other a plastic plate. The amount of pressure applied ranges from 3 to 6 N [4]. Mammography is an uncomfortable procedure for women, and in some cases the breast does not return to its normal state. Conventional mammography is limited by the small size of the breast tissue in younger ages [4]. Because of the harmful effects that x-ray waves have on the human body, new optical imaging

*Corresponding Author Email: *aesmaeli@aeoi.org.ir* (A. Esmaeli)

Please cite this article as: Y. Noori shirazi, A. Esmaeli, M. B. Tavakoli and F. Setoudeh, Improving 3-D Imaging Breast Cancer Diagnosis Systems Using a New Method for Placement of Near-infrared Sources and Detectors, International Journal of Engineering (IJE), IJE TRANSACTIONS C: Aspects Vol. 33, No. 6, (June 2020) 1105-1113

systems have been receiving great attention [5]. In addition to mammography and clinical examinations, sonography and MRI (magnetic resonance imaging) are other imaging methods. MRI images provide anatomical information from the examined breast tissue, but functional information of the breast tissue is required for diagnosing breast cancer. In some special cases, CT (computed tomography) is used, and PET (positron emission tomography) imaging is also used; this imaging method, however, requires the injection of radioactive substances [6- 8]. Clearly, using near-infrared light for a more accurate diagnosis of abnormal areas with fewer ill effects is necessary.

Research using light for imaging breast tissue was conducted in a dark room [9], and the shadows of large tumors in breast tissue were examined. Near-infrared lights can penetrate tissue, and hemoglobin concentration and oxygen saturation levels can be computed using the measurement data [10]. The results of such research, however, were not satisfactory because of the increasing temperature of the patients' skin [9]. Nevertheless, the investigations [11, 12] were a major step towards using near-infrared light to examine the optical properties of tissue. It has been indicated that the amount of hemoglobin in tumors is two to three times that of in healthy tissue [11, 12]. The use of near-infrared lights to image soft tissues (such as the breast) has received much attention due to its non-invasive and non-ionization properties [13, 14].

2. OPTICAL IMAGING

2. 1. Optical Image System The optical imaging system consists of two parts: hardware and software [14]. The hardware part of the system consists of optical detectors and sources that surround the physiological tissues. It is responsible for providing the required raw data for the software part of the system. The software part is responsible for reconstructing an image from raw data within the shortest possible time. The optical imaging system has been designed based on near-infrared light emission in tissue, and it has been used to monitor oxygen levels inside the tissue. In this imaging system, near-infrared light with the wavelength of 650 to 900 nm is radiated by optical fibers that surround the area under consideration; then, the intensity of the refracted light is received by other detectors [15]. The reason for using the stated wavelength is that water is the main absorbent of light in ultraviolet waves, proteins, and long infrared wavelengths, , hence a light beam cannot penetrate the tissue significantly. In the near-infrared spectral range, however, light can penetrate tissue more deeply due to the higher light scattering. The difference in the absorbed spectrum is an effective factor in identifying arterial blood (oxygenated hemoglobin) from venous blood (deoxygenated hemoglobin) [15-18].

The light emission in tissue is affected by the optical properties of the tissue, and the elements of the tissue have different absorption and scattering properties (μa, μs) in different wavelengths of near-infrared light. Therefore, the intensity of the reflected light can well describe the optical properties of the tissue under consideration. The most important objectives in optical imaging are to estimate and reconstruct the optical properties (μa, μs) of tissue by radiated light and to measure the reflection of this light in the area under consideration [19]. This method has a great number of usages in the fields of mammography and imaging from the head of newborn babies.

Analytical and numerical methods are used to solve diffusion equations of light in tissue. Analytical methods are quicker than numerical methods. In general, analytical methods can be used in the simple medium, and numerical methods can be used in complex and non-homogenous mediums. For this reason, numerical methods are now more frequently used. One numerical method for forward solving of a problem is the finite element method [20]. With this method, the surface under consideration is divided into small elements, and then absorption and scattering coefficients are calculated for each element. However, since image reconstruction is an ill-behaved problem (small changes in data can lead to great changes in output), regularization methods can be used to obtain a stable solution [21]. In non-linear and non-stochastic conditions, there are two different optimization methods for image reconstruction: the gradient-based method [21, 22] and the Newton method [23], both of which are repeatitive methods of image reconstruction. The advantage of the gradient-based optimization method is that it has minimum complexity; its drawback, however, is that the number of repetitions of the algorithm for solution convergence is high. The Newton method reconstructs an image with fewer repetitions, but it has high complexity compared with the gradient-based method. Thus, the NIRFAST image reconstruction toolbox was embedded in MATLAB software in order to remove the high complexity. In this research, the use of formula and manual problem-solving were avoided, and the image reconstruction toolbox was employed instead.

2. 2. Imaging Technique As Figure 1 shows, to obtain an image, the patient must lie on the bed [5], and the breast is placed through the hole in the bed in a ring of near-infrared light-emitting diodes. The patient must not be moved during the imaging process. Since breast tissue is not compressed in this imaging system, the patient does not feel any pain [5]. Beneath the bed, an array of near-infrared light sources and detectors are placed in a ring that makes direct contact with the breast tissue. At first, the array moves vertically where it approaches the hole in the bed. Then, the array moves

circularly where the breast tissue sits in the hole. All vertical and circular movements of the array of near-infrared light sources and detectors are controlled by the LAB view software in a computer. The data is measured within 30 seconds, and the amplitude and phase are calculated and transferred to the image reconstruction toolbox in the MATLAB programming environment until an optical image of the tissue is reconstructed numerically by the finite element method [5]. With this method, the surface under consideration is divided into small elements that are considered as triangle meshes, in which each mesh consists of some nodes. Then absorption and scattering coefficients are calculated for each element. However, regularization methods can be used to obtain a stable solution as image reconstruction is an ill-behaved problem (small changes in data can lead to great changes in output),.

2. 3. Image Reconstruction by Near-infrared Lights As shown in Figure 2, one 15 × 10 mm cylinder was detected within a 50 × 50 mm cylinder using the 3-D Newton reconstruction algorithm [24]. As shown in this figure, one ring of 16source and four rings of 16-detector were used in which two of the detector rings were placed above and below the source [24]. Figure 3 shows a reconstructed image by near-infrared light [25]. Figure 3(a) is an image before reconstructing, and Figure 3(b) is a reconstructed image.

To obtain a reconstructed image, near-infrared light was first radiated on the breast tissue by the sources, and then refracted light was measured by detectors.

Figure 1. Patient bed [5]

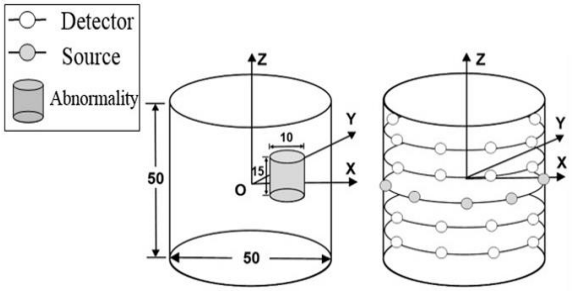

Figure 2. Location of detectors, sources and abnormality [24]

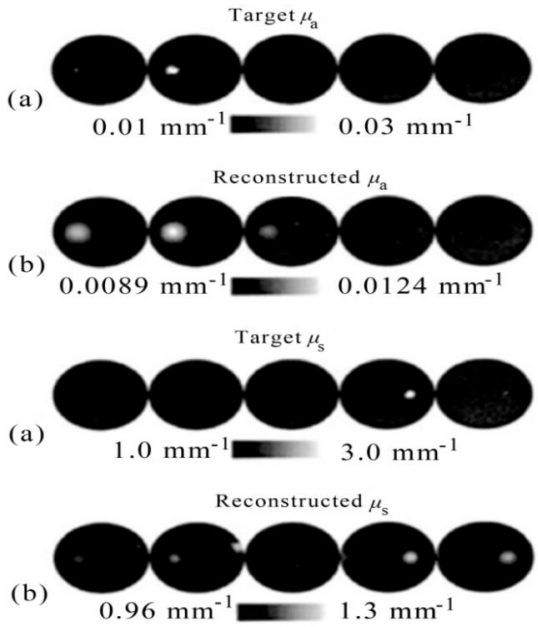

Figure 3. Absorption coefficient (μa) and scattering coefficient (μs) before and after image reconstruction in different layers; (a) is an image before reconstructing, and (b) is a reconstructed image [25]

Because of the difference between the amplitude and phase of the radiated and the measured light, the reconstruction operation was conducted (once based on μa, and once based on μs). The results showed that the reconstruction operation was repeated nine times due to low technology on that time [25], and the output image was placed in the form of two-dimensional layers. The results also showed that the provided algorithm could display rapid and reliable images from optical properties within the tissue., The costs and the destructive effects of this method on tissue are lower than those from other methods [25]. In another research conducted in [26], near-infrared light technology was used to detect small objects. In this study, a cylindrical area with a height of 109 mm and diameter of 84 mm was considered as a reference area, and the abnormal area was placed as a small cylinder close to the reference cylinder

circumference [26]. The small cylinder represented breast tumors that required a more exact diagnosis. As discussed in [26], the reconstructed images based on μs are more accuratet than the reconstructed images based on μa. Today, the reconstruction of optical images with minimum distortion and noise has garnered the attention of many researchers, and it is used in clinical and diagnostic applications. In the present paper, a new placement of light sources and detectors surrounding the tissue is proposed. Using this placement, abnormal areas are detected with a very low error rate, and good results have been obtained when there are two abnormal areas in different parts of breast tissue.

3. PROPOSED METHOD

3. 1. Proposed Method for Diagnosing Tumor in Reconstructing Image In this article, human breast cancer samples were examined due to the inaccessibility of a 3-D imaging system by near-infrared lights. Such experiments should be conducted at frequent times to obtain more accurate reconstructed images. The working trend in the process of reconstructing an image is shown in Figure 4. As shown in this figure, the first step is to construct a reference area in the form of a cylinder using NIRFAST toolbox. For this area, optical characteristics (μa, μs) are not defined, and the breast tissue is placed in the space of the cylinder. In this article, this space was considered as triangle meshes, and each mesh consists of some nodes. The height of the cylinder was 50 mm, its radius was 25 mm, and its center coordinate was (0, 0, 0). Since the height and radius of the cylinder are considered as a constant value, the number of nodes can be increased or decreased by changing the distance between the nodes. Certainly, the quality of the reconstructed image improves when the numbers of nodes is increased, but reconstruction operation time is also increased. As distance between the nodes is suggested by the NIRFAST toolbox considering the height and radius of the cylinder, the reconstruction operation optimizes both the time and quality of the reconstructed image. In the next step, the sources and detectors are placed in proper points of the cylinder circumference; in this article, three 16-source rings were placed in Z = 3, 0, and -3, and eight 16-detector rings were placed in Z = 1, 2, 4, 5, -1, -2, -4, and -5. In the next step, the breast tissue is constructed by the NIRFAST toolbox in the form of a sphere and includes the entire cylinder. The optical specifications are considered for it, and then a small sphere is considered within the breast tissue. This sphere is the abnormal area (tumor), the optical characteristics of which must differ from the optical characteristics of the breast tissue. In this step, number of abnormal area can be increased more, for example, one breast tissue with two abnormal areas. In the next step, near-infrared lights are radiated through sources to the breast tissue, and detectors receive the intensity of the refracted light. The breast tissue consists of different components, each of which has different μa and μs.

When a source radiates the near-infrared light to the tissue, the intensity of the refracted light is measured by 128 detectors with different amplitudes and phases. Ultimately, 6144 bits of data with different amplitudes and phases are measured by the detectors, and the NIRFAST toolbox reconstructs the image. At the end, the level of overlap between the reconstructed and initial images are examined through coding in the MATLAB programming environment which is good for evaluating of accuracy of the reconstruction.

3. 2. Calculating Percentage of Overlap Between Reconstructed Image and Initial Image In this problem, the space is a cylinder with the height of 50 mm and radius of 25 mm. The optical properties of the breast tissue are μ_a=0.01 and μ_s=1. The abnormal area was placed as a sphere with a radius of 8 mm, μ_a=0.02, and μ_s=1 in the coordinates of (13, 0, 0). In the reconstructed image, μ_a=0.02 to 0.009 were found, indicating that the abnormal sphere in the reconstructed image was seen with a shadow margin. In the first step, the numbers of nodes in the main sphere were calculated in the initial image.

In fact, they are the numbers of nodes with μ_a=0.02. In the next step, the boundary of μ_a was delineated in the reconstructed image. This boundary was selected in order to have the least difference between the number of nodes in it and the number of nodes in the main abnormal sphere. Therefore, the value of μ_a=0.01 to0.02 with step=0.0001 was changed, and the number of

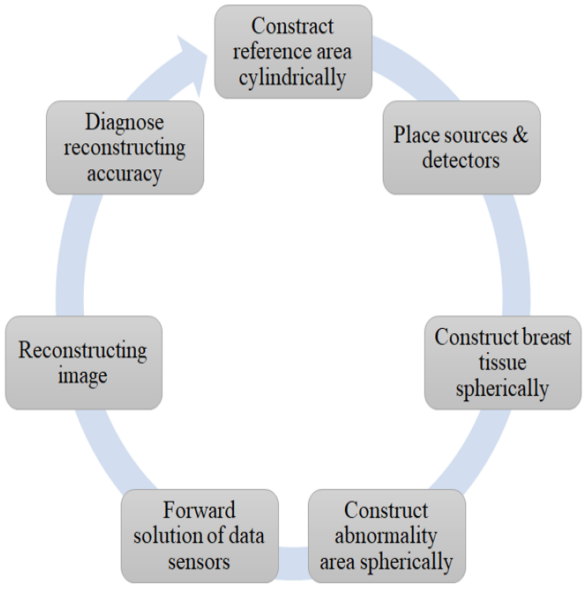

Figure 4. Working trend in the process of reconstructing images

nodes within this boundary with the desired μ_a was calculated. Then the difference between the obtained nodes and the numbers of nodes in the main sphere were saved in variable *d*. At the end of this loop, the minimum value of *d* in variable *m* and its μa in variable *a* were saved. Then in one loop, those nodes with a μ_a greater than *a* were saved in variable *b*. In this loop, the number of nodes for *b* were calculated and saved in variable *p*, and the number of nodes for *b* that have coordinates in the main abnormal sphere were calculated and saved in a variable *q*. Then, the percentage of overlap was calculated using Equation (1).

$$percentage\ of\ overlapping\ = \frac{p}{q} \times 100 \quad (1)$$

3. 3. Presentation of Optimal Location Model

Based on the repeated experiments done in this research using MATLAB software, with the presented optical imaging system, a more accurate diagnosis of an abnormal area depends on the location of the sources and detectors. Thus, the rings of light sources and the rings of light detectors were placed in the selective height of the cylindrical wall. Then, the reconstructed image of the tissue and abnormal area were produced. Next, based on the coding presented in the MATLAB programming environment, the reconstructed image was compared with the initial image in terms of overlapping. Experiments that showed at least 98% overlapping between the reconstructed image and the initial image was considered as the statistical sample, and based on this sample, an optimal location model was presented. In this model, the optimal height of the tumor was first defined; then, a ring of near-infrared light sources was placed at the same height in the cylindrical wall, and other rings of sources and detectors were placed slightly higher or lower than the optimized distance. In this model, the location of the tumor was at the expected optimal height x^*, but it may be placed higher or lower than its real location; thus, its accurate location can be modeled by Equation (2):

$$\pi(x) = w_1 E(x^*) - w_2 E(x^* - x) - w_3 E\,(x - x^*) \quad (2)$$

where *x** is a random variable representing the optimal location of the tumor, *X* is the selective location of the tumor, *π(x)* is the exact selection of the tumor location, *E(x*)* is the expected value of the optimal location, *E(x*- x)* is the expected value of the selective location which is lower than the optimal location of the tumor, and *E(x-x*)* is the expected value of the selective location which is higher than the optimal location of the tumor. Furthermore, w_1 is the ratio of the tumor placed in the optimal location, w_2 is the ratio of the tumor placed lower than the optimal location, and w_3 is the ratio of the tumor placed higher than the optimal location. If G(x) is in the form of Equation (3), then Equation (4) will be obtained from Equations (2) and (3). However, if *x** is known, Equation (5) will be obtained.

$$G(x) = w_2 E(x^* - x) + w_3 E(x - x^*) \quad (3)$$

$$\pi(x) = w_1 E(x^*) - G(x) \quad (4)$$

$$w_1 E(x^*) = w_1 \mu \quad (5)$$

In Equation (5), μ is the average. If x^* is not known, Equation (6) will be obtained.

$$\acute{G}(x) = \frac{dG(x)}{dx} = 0 = w_2 E\delta\,(x^* - x) + w_3 E\delta(x - x^*) \quad (6)$$

Asthe derivative functionshows the variation slope, the expected value of variations that is called E(δ) can be considered equivalent to the derivative; hence, Equations (7) and (8) are obtained as follows.

$$E\delta(x^* - x) = P(x^* - x \geq 0) = P(x^* \geq x) = 1 - F(x) \quad (7)$$

$$E\delta(x - x^*) = P(x - x^* \geq 0) = P(x^* \leq x) = F(x) \quad (8)$$

In Equations (7) and (8), P(x* ≥ x) is the probability that the optimal location is higher than the selective location, and P(x* ≤ x) is the probability that the optimal location is lower than the selective location. Equations (9) through (13) are obtained from Equation (6).

$$w_2\big(1 - F(x)\big) + w_3 F(x) = 0 \quad (9)$$

$$\Longrightarrow w_2 = (w_2 - w_3)F(x) \quad (10)$$

$$\Longrightarrow F(x) = \frac{w_2}{w_2 - w_3} = \beta \quad (11)$$

$$\Longrightarrow x^* = F^{-1}(\beta) \quad (12)$$

$$\Longrightarrow x^* = inf\{x \parallel F(x) \geq \beta\} \quad \& \quad \beta = \frac{w_2}{w_2 - w_3} \quad (13)$$

Considering the normal distribution function, x^* is the same as in Equation (14), in which μ is the average, σ is the standard deviation, and z is the standard normal. Considering ϕ(z) = P(Z ≤ z), Equation (15) is obtained, and Equation (16) is resulted from Equations (12) and (15), where Z_β is the confidence interval.

$$x^* = \mu + \sigma z \quad (14)$$

$$Z_\beta = \phi^{-1}(\beta) \rightarrow P\big(x^* < \mu + Z_\beta \sigma\big) = \phi\big(Z_\beta\big) = \beta \quad (15)$$

$$x^* = \mu + Z_\beta \sigma \quad (16)$$

The values of the calculated parameters of the optimal location model based on the considered statistical sample are shown in Table 1.

Based on Table 1, the optimal location of the tumor was defined at the height of Z=0. Thus, three 16-source

TABLE 1. Calculated values of the location model parameters.

Parameter	Value
w_2	3
w_3	1
β	$\beta = \frac{w_2}{w_2 - w_3} = 1.5$
$\phi^{-1}(\beta)$	$z_{1.5} = 0.9332$
μ	-0.36
σ	0.54626
x^*	$x^* = \mu + Z_\beta \sigma \simeq 0$

rings in Z= 3, 0, and -3 and eight 16-detector rings were placed in Z= 1, 2, 4, 5, -1, -2, -4, and -5. Image reconstruction was conducted with this placement of sources and detectors, and good results were obtained.

4. SIMULATION AND RESULTS

4. 1. Simulation of Previous Research The latest and most important investigations into the alignment of resources and detectors, as far as we know, were carried out in 2003 by Dehghani et al. [25, 26]. In the following years, the research team focused on designing and improving the NIRfast toolbox, and later on embarked on a device manufacturing project that was able to implement their design and become a Knowledge-Based Company at Dartmouth College, US thathas been working on breast tissue imaging to detect tumors. But the image reconstructed by their design is not very accurate. To improve the reconstructed images of their designs, they looked into various numerical solutions and methods of responding to convergence, upgrading the software of their design and neglecting the hardware. By conducting experiments, we found that by increasing the number of measured data, we could reduce the effect misconducted behavior had on reversing the problem and improve the accuracy of the reconstructed images. The number of sources and detectors can be increased to increase the amount of measured data, but these sources and detectors need to be well positioned, so we provide an optimal location model for locating sources and detectors. Another reason for not continuing their research on methods of increasing and rearranging resources and detectorsmay have been due to higher material costs, because increasing and rearranging sources and detectors is bounded by the price of machinery which are used for such purposes

At first, the conducted research in reference [24] was simulated. In this case, the geometrical and optical properties of the cylinder were 50 × 50 mm with μa=0.01 and μs=1, and the abnormal area was located as a sphere with a radius of 8 mm in the coordinates (13, 0, 0) with μa= 0.02 and μs=1. The locations of the sources and detectors in this case were consistent with the findings in [24], such that one 16-source ring in Z=0 and four 16-detector rings were placed in Z=7, 14, -7, and -14. The result of image reconstruction is shown in Figure 5.

Figure 5 is the final image of the 3-D analysis based on the absorption coefficient. In this figure, the top right image is the x-axis and the bottom-left image is the y-axis and the bottom-right image is the z-axis, and the top-left image is a 3-D output image. The right volume of each of these axes is to represent the image at different levels of each axis.

The lower volume of each of these axes is the threshold image, and the lower volume of the output image, called the alpha, is a coefficient, which displays better resolution by moving this volume (these images can be observed based on μa and μs and altogether). In the following, the presented coding in MATLAB was used to determine image overlap before and after reconstruction, and the level of overlap was 72.63%. In [26], the process was performed according to the given data, and the overlap level was 78.57%.

4. 2. Simulation of Proposed Method in the Present Research Image reconstruction was done based on the proposed method with the coordinates of the sources and detectors such that three 16-source rings were placed in Z= 3, 0, and -3 and eight 16-detector rings were placed in Z= 1, 2, 4, 5, -1, -2, -4, and -5. Figure 6 shows the reconstructed image in this case. It was found intuitively by comparing the two reconstructed images in Figures 5 and 6 that an abnormal sphere is better recognized using the proposed method. Then, the coding presented in MATLAB was used to determine image overlap before and after reconstruction, and the level of overlap was determined to be 99.53%.

Figure 7 is the reconstructed image of breast tissue with two abnormal areas that were placed symmetrically at the same height. The levels of overlap were 99.53% and 99.76% for the first and second abnormal areas, respectively. Figure 8 is the reconstructed image of breast tissue with two abnormal areas that were placed symmetrically at different heights, and the overlap level was 99.76% and 63.88% for the first and second abnormal areas, respectively. As shown in Figures 7 and 8, the proposed method performs well when two abnormal areas are present. It is worth mentioning that the closer the abnormal area to the sources center and the detectors, the greater the accuracy of detection. That is, if the radiologist takes an image of the patient and suspects a tumor, he or she can continuously move the

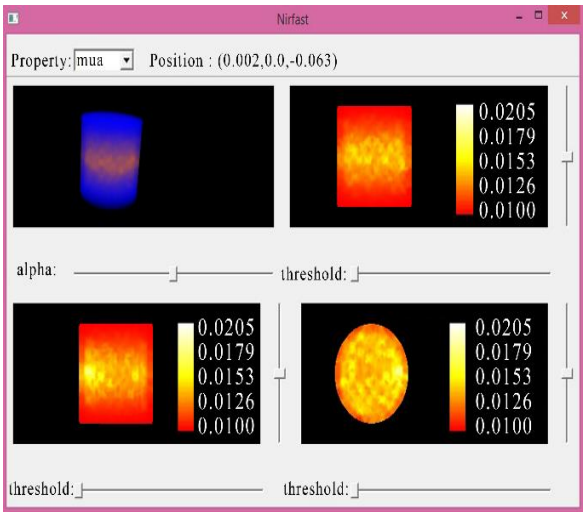

Figure 5. 3-D reconstructed image based on the conducted research in [24]

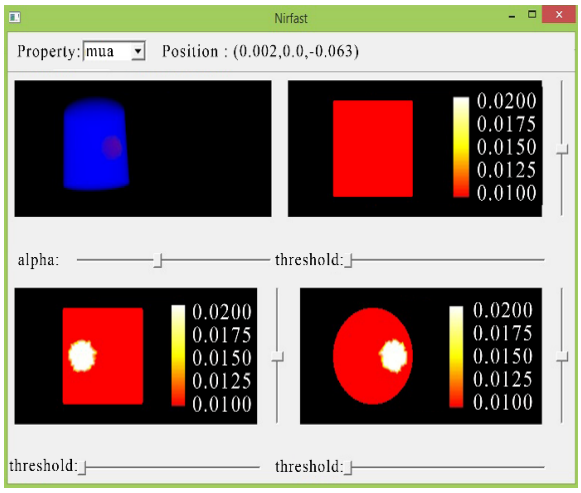

Figure 6. 3-D reconstructed image in the proposed method

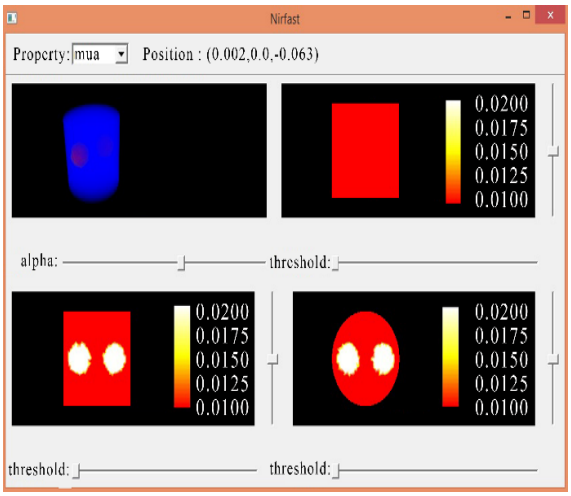

Figure 7. 3-D reconstructed image of two abnormal areas in the same height (Z)

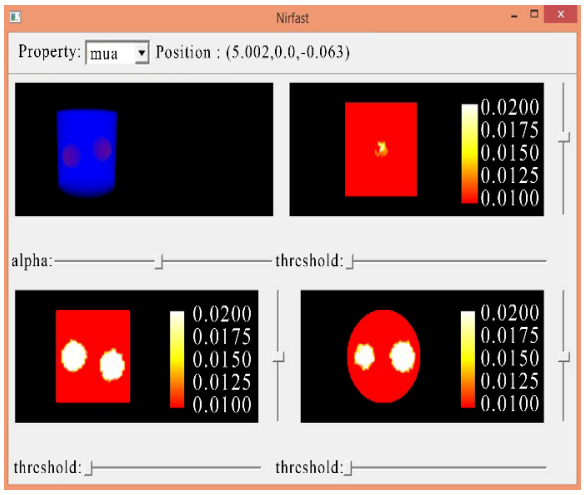

Figure 8. 3-D reconstructed image of two abnormal areas in different height (Z)

cylinder where the sources and detectors are fixed to the wall and repeat the imaging process till the tumors are close enough to the resource's center and detectors and more accurately diagnosed.

Table 2 shows the results of experiments for different locations of abnormal areas in breast tissue. Based on these results, reconstructed 3-D images of breast tissue were significantly improved by near-infrared lights. This can be greatly helpful at diagnosing breast cancer more accurately.

5 .CONCLUSION

As was evident in the simulations, by changing the location of the sources and detectors, better results were achieved both intuitively and quantitatively. In this article, an optimal location model was used to more accurately detect the anomaly area presented by the same research team, and it was observed that by locating the sources and detectors in the same sites we proposed, the area could be found with 21% higher accuracy compared to other previous work. On the other hand, image reconstruction is an inverse problem, and any inverse problem is misconduct behavior. To eliminate the effects of misconduct behavior, the number of measured data had to be increased, which was done by adding a number of sources and detectors. Also, the accuracy of the two anomalies, whose coordinates were different in some axis, was evaluated and good results were obtained. As a result, more accurate detection and obtaining a higher resolution image in 3-D reconstruction of the breast tissue by near-infrared light is correlated with the precise location of sources and detectors. This design can be used to tackle

TABLE 2. Experiment results for different locations of abnormal area

	Spectrum properties	Spectrum properties of abnormalities	Size of the cylinder	Place of abnormalities	Percentage of overlapping
[24]	μa = 0.01 μs = 1	μa = 0.02 μs = 1	R=25 H=50	(13,0,0) R=8	72.63%
[26]	μa = 0.01 μs = 1	μa = 0.02 μs = 1	R=25 H=50	(13,0,0) R=8	78.57%
Figure 6	μa = 0.01 μs = 1	μa = 0.02 μs = 1	R=25 H=50	(13,0,0) R=8	99.53%
Figure 7	μa = 0.01 μs = 1	μa = 0.02 μs = 1	R=25 H=50	(13,0,0) R=8 (-13,0,0) R=8	A=99.53% B=99.76%
Figure 8	μa = 0.01 μs = 1	μa = 0.02 μs = 1	R=25 H=50	(13,0,0) R=8 (-13,0,-5) R=8	A=99.76% B=63.88%

important issues such as: non-invasive property, relieving pressure from the breast tissue, decreasing pain, higher accuracy of detection, elimination of unnecessary biopsy and no need to inject radioactive material to better detect breast cancer, and help to better detect breast cancer through future NIR imaging.

6. REFERENCES

1. Nirouei, M., Pouladian, M., Abdolmaleki, P. and Akhlaghpour, S., "Chaos analysis of breast masses on dynamic magnetic resonance mammography", IEEE International Conference on Signal and Image Processing (ICSIP), (2016), 300-304.
2. Porto-Mascarenhas, E. C., Assad, D. X., Chardin, H., Gozal, D., Canto, G. D. l., Acevedo, A. C. and Guerra, E. N. S., "Salivary biomarkers in the diagnosis of breast cancer: A review", Critical reviews in oncology/hematology, (2017), 62-73.
3. Kenny, L. M., Orsi, F. and Adam, A., "Interventional radiology in breast cancer", ***The Breast***, Vol. 35, (2017), 98-103.
4. Jackson, V. P., Hendrick, R. E., Feig, S. A. and Kopans, D. B., "Imaging of the radiographically dense breast", ***Radiology***, Vol. 188, No. 2, (1993), 297-301.
5. Keating, J., Tchou, J., Okusanya, O., Fisher, C., Batiste, R., Jiang, J., Kennedy, G., Nie, S. and Singhal, S., "Identification of breast cancer margins using intraoperative near-infrared imaging", ***Journal of Surgical Oncology***, Vol. 113, No. 5, (2016), 508-14.
6. Apostolakis, S., Ioannidis, A., Tsioga, G., Papageorgiou, K. and Velimezis, G., "A systematic investigation of sclerosing mesenteritis through CT and MRI", ***Radiology Case Reports***, Vol. 11, No. 4, (2016), 299-302.
7. Khosravi, M. and Hassanpour, H., "Image denoising using anisotropic diffusion equations on reflection and illumination components of image", ***International Journal of Engineering-Transactions C: Aspects***, Vol. 27, No. 9, (2014), 1339-1348.
8. Hajihashemi, V. and Borna, K., "An adaptive hierarchical method based on wavelet and adaptive filtering for MRI denoising", ***International Journal of Engineering-Transactions A: Basics***, Vol. 29, No. 1, (2016), 31-9.
9. Cutler, M., Cutler, M. and Cutler, M. M., "Transillumination as an aid in the diagnosis of breast lesions", ***Surgery Gynecol Obstet***, Vol. 48, (1929), 721-9.
10. Rolfe, P., "In vivo near-infrared spectroscopy", ***Annual Review of Biomedical Engineering***, Vol. 2, No. 1, (2000), 715-54.
11. Jobsis, F. F., "Noninvasive, infrared monitoring of cerebral and myocardial oxygen sufficiency and circulatory parameters", ***Science***, Vol. 198, No. 4323, (1977), 1264-7.
12. Troy, T. L., Page, D. L. and Sevick-Muraca, E. M., "Optical properties of normal and diseased breast tissues: prognosis for optical mammography", ***Journal of Biomedical Optics***, Vol. 1, No. 3, (1996), 342-56.
13. Zhou, W., Lu, J., Zhou, O. and Chen, Y., "Ray-tracing-based reconstruction algorithms for digital breast tomosynthesis", ***Journal of Electronic Imaging***, Vol. 24, No. (2), (2015), 023028.
14. Rahim, R. A., Leong, L. C., Chan, K. S. and Pang, J. F., "Data acquisition process in optical tomography: Signal sample and hold circuit", 1st International Conference on Computers, Communications, & Signal Processing with Special Track on Biomedical Engineering, IEEE, (2005), 189-192.
15. Wilson, B. C. and Jacques, S. L., "Optical reflectance and transmittance of tissues: principles and applications", ***IEEE Journal of Quantum Electronics***, Vol. 26, No. 12, (1990), 2186-99.
16. Kumar, S., Kumar, V., Abhilasha, A., Garg, M. and Jain, D., "Fourier transform infra- red spectroscopic studies on epilepsy, migraine and paralysis", ***International Journal of Engineering-Transactions B: Applications***, Vol. 23, No. 3&4, (2010), 277.
17. Gholami, A. and Hassanpour, H., "Finger vein recognition in radon space using local entropy thresholding and common spatial pattern", ***International Journal of Engineering-Transactions A: Basics***, Vol. 28, No. 1, (2014), 25-34.
18. McBride, T. O., "Spectroscopic reconstructed near infrared tomographic imaging for breast cancer diagnosis", Doctoral dissertation, Dartmouth College, 2011.

19. Kolehmainen, V., "Novel approaches to image reconstruction in diffusion tomography", Kuopio, Finland, Kuopion yliopisto, 2001.
20. Arridge, S. R., Schweiger, M., Hiraoka, M. and Delpy, D. T., "A finite element approach for modeling photon transport in tissue", ***Medical Physics***, Vol. 20, No. 2, (1993), 299-309.
21. Hielscher, A. H. and Bartel, S., "Use of penalty terms in gradient-based iterative reconstruction schemes for optical tomography", ***Journal of Biomedical Optics***, Vol. 6, No. 2, (2001), 183-93.
22. Hielscher, A. H., Klose, A. D. and Hanson, K. M., "Gradient-based iterative image reconstruction scheme for time-resolved optical tomography", ***IEEE Transactions on Medical Imaging***, Vol. 18, No. 3, (1999), 262-71.
23. Hanke, M. and Hansen, P. C., "Regularization methods for large-scale problems", ***Surv, Math, Ind***, Vol. 3, No. 4, (1993), 253-315.
24. Jiang, H., Xu, Y. and Iftimia, N., "Experimental three-dimensional optical image reconstruction of heterogeneous turbid media from continuous-wave data", ***Optics Express***, Vol. 7, No. 5, (2000), 204-9.
25. Dehghani, H., Pogue, B. W., Poplack, S. P. and Paulsen, K. D., "Multiwavelength three-dimensional near-infrared tomography of the breast: initial simulation, phantom, and clinical results", ***Applied Optics***, Vol. 42, No. 1, (2003), 135-45.
26. Dehghani, H., Pogue, B. W., Shudong, J., Brooksby, B. and Paulsen, K. D., "Three-dimensional optical tomography: resolution in small-object imaging", ***Applied Optics***, Vol. 42, No. 16, (2003), 3117-28.

Persian Abstract

چکیده

هدف از این پژوهش بهبود سامانه عکسبرداری سه بعدی به وسیله انتشار نور نزدیک مادون قرمز در بافت پستان، جهت تشخیص دقیقتر تومور می‌باشد. بر اساس آزمایشات که در این تحقیق انجام گرفته شد، این نتیجه حاصل شده است که، تشخیص دقیقتر ناحیه ناهنجاری در این سیستم عکس‌برداری، به محل قرارگیری منابع و آشکارسازها بستگی دارد، لذا با ارائه یک مدل مکان‌یابی بهینه شده، موقعیت مناسب‌تری، جهت قرارگیری منابع و آشکارسازها، پیشنهاد داده شده است. در این مقاله، به دلیل عدم دسترسی به دستگاه عکس برداری سه بعدی بوسیله نور نزدیک مادون قرمز، از نمونه‌های انسانی مبتلا به سرطان پستان استفاده نشده است، و از آنجایی که، برای بدست آوردن تصویر بازسازی شده‌ی دقیقتر، آزمایشات می‌بایست به دفعات زیادی انجام می‌گرفت، لذا برای ارزیابی این روش پیشنهادی، از جعبه ابزار بازسازی تصاویر نوری NIRFAST ۷.۲ که در محیط برنامه-نویسی نرم‌افزار MATLAB کدنویسی شد، استفاده شده است، سپس نتایج به دست آمده، با نتایج به دست آمده از مقالات مشابه قبلی، مقایسه شده است، نتایج به دست آمده نشان داد که با چینش پیشنهادی منابع و آشکارسازها، ناحیه ناهنجاری با خطای بسیار پایین‌تر تشخیص داده شده است، همچنین این چینش پیشنهادی منابع و آشکارسازها، نتیجه مطلوبی را در تشخیص همزمان دو ناحیه ناهنجاری ارائه داده است.